Data in Brief 63 (2025) 112118

Contents lists available at ScienceDirect

Data in Brief

journal homepage: www.elsevier.com/locate/dib

Data Article

Experimental dataset on wave–structure interaction in a sloshing tank with a flexible floating body

Francisco Bernardo[a,b,*], Moisés Brito[a,b], Rui M.L. Ferreira[c], João Leal[d]

[a] UNIDEMI, Department of Mechanical and Industrial Engineering, NOVA School of Science and Technology, Caparica, 2829-516, Portugal
[b] Laboratório Associado de Sistemas Inteligentes, LASI, Portugal
[c] CERIS, Instituto Superior Técnico, Universidade de Lisboa, Lisbon, 1049-001, Portugal
[d] Faculty of Engineering and Science, University of Agder, Kristiansand, 4630, Norway

ARTICLE INFO

Article history:
Received 17 April 2025
Revised 12 August 2025
Accepted 24 September 2025
Available online 30 September 2025

Dataset link: Experimental Dataset on the interaction of sloshing tank waves with a flexible floating body (Original data)

Keywords:
Sloshing tank
Fluid-structure interaction
CFD
Flexible Floating Structure

ABSTRACT

There is a critical need for robust validation methods in Computational fluid Dynamics (CFD), particularly for innovative applications involving fluid-structure interactions (FSI). This work presents a comprehensive dataset, including velocity vectors and wall-pressure measurements, obtained from a purpose-built experimental sloshing tank. The design of the tank was CFD-conscious and specific for validation purposes, i.e. choices on operation principles, dimensions, materials and optical access were made to facilitate CFD model implementation while constituting a challenging fluid mechanics problem involving floating flexible bodies. The construction process, the instrumentation, and data collection methods are explained in detail. Though liquid sloshing in a tank is a well-studied subject, this work emphasizes the influence of the flexible floating body on the velocity field and wall-pressure associated to the waves formed by the sloshing rotation of the tank. This dataset allows for validating and improving CFD codes for simulating FSI of flexible bodies. In particular, it provides insights for refining simulations of waves interacting with Very Flexible Floating Structures

* Corresponding author.
E-mail address: fr.bernardo@campus.fct.unl.pt (F. Bernardo).

https://doi.org/10.1016/j.dib.2025.112118

(VFFS), like the case of offshore Floating Photovoltaic cells (FPV).

Specifications Table

Subject	Hydrodynamics
Specific subject area	Fluid-Structure interaction with highly elastic structures
Type of data	High-speed video (raw images and processed video), Velocity vectors (two planar components) from Particle Imaged Velocimetry (PIV), Free surface height, pressure on the tank's wall, tank's position over time.
Data collection	All the data was taken from waves created in an in-house built sloshing tank. The sloshing tank dimensions are 1 × 0.6 × 0.2 m. There are three main data collecting systems: 1. High speed camera (Allied Vision BONITO CL400b), an LED light sheet and in-house software for Particle Image Velocimetry analysis (PIV) and free surface detection; 2. Five Pressure transducers for recording pressure at various locations on the tank walls; 3. Rotary encoder recording the tanks position.
Data source location	Data collected at the Department of Mechanical and Industrial Engineering at NOVA School of Science and Technology, Caparica, Lisbon. Instrumentation owned by NOVA School of Science and Technology and by Instituto Superior Técnico.
Data accessibility	Repository name: Zenodo Data identification number: 10.5281/zenodo.15223412 Direct URL to data: https://zenodo.org/records/15223412 Instructions for accessing these data: Download and unzip
Related research article	None, to be published in the future

1. Value of the Data

- The experimental tank was built with the purpose of obtaining experimental data for the validation of CFD numerical codes, applied to simulating maritime waves interacting with Very Flexible Floating Structures (VFFS).
- The dataset provides high accuracy data including flow velocity fields, wall pressures and free-surface/body deformations over time, essential for validating CFD models of FSI, particularly involving floating and very flexible structures.
- The dataset can also provide physical insights on sloshing dynamics when floating bodies are present.

2. Background

The purpose of this work is to provide data for the validation of CFD codes for the simulation of FSI of oceanic waves and very flexible floating structures. A pertinent application is the design and testing of offshore Floating Photovoltaic cells (FPV). Existing datasets on FSI involving flexible bodies, acquired in experimental wave flumes, are not sufficiently detailed to allow for comparison with CFD, are not reproducible by CFD, for lack of critical information, or do not cover the range of phenomena necessary for CFD validation. This justifies the decision to manufacture a purpose-built, CFD-conscious, sloshing tank to generate a more diverse and accurate dataset for validation including planar velocity vectors and wall-pressure measurements.

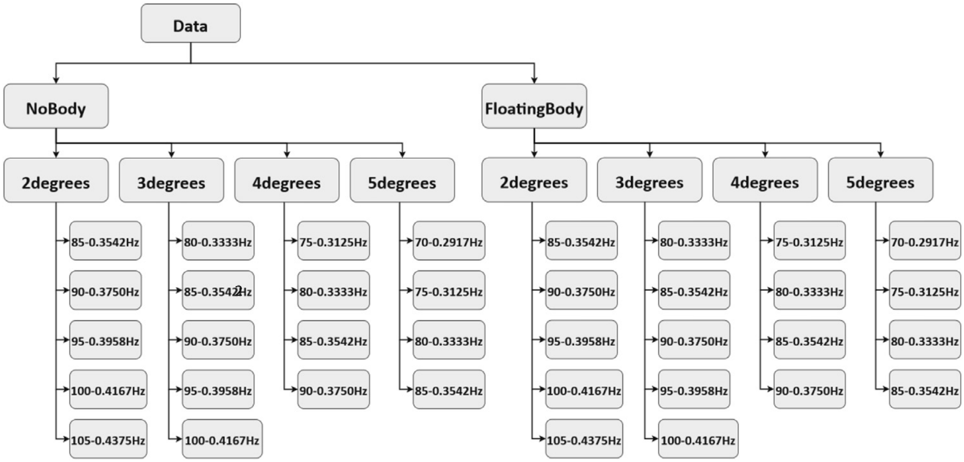

Fig. 1. Dataset folder layout.

3. Data Description

The dataset consists of two main groups of experiments, with and without a floating body. The data are in the “FloatingBody” and “NoBody” folders respectively (see in Fig. 1).

The experimental runs without the floating body are preliminary and important to set a benchmark for the fluid flow as a simple sloshing problem. They may be of interest to the community studying sloshing behavior in liquids. However, the focus of the dataset is the FSI with very flexible floating bodies.

To obtain a comprehensive dataset for validation, several sloshing conditions were applied on the experimental runs, both with and without the floating body. Conditions vary by changing the amplitude and frequency of the sloshing motion. Data corresponding to four different amplitudes is stored in folders “2degrees”, “3degrees”, “4degrees” and “5degrees” (see Fig. 1). For each amplitude, there were four or five frequencies analyzed for a total of 18 sloshing conditions.

The naming of the folders inside each amplitude folder is “motorRPM-RotationFrequency”. As an example for a case with an amplitude of 2 degrees and motor RPM set as 85, the folder is named “2deg_85–0.3542Hz” located inside the “2degrees” folder. Fig. 1 shows the folder layout of the dataset.

For each sloshing condition there were two separate recordings, one capturing the entire tank (at 100 fps) and another capturing only the lower left corner of the tank for Particle Image Velocimetry (PIV) processing, at 405 fps. Inside each sloshing condition folder of Fig. 1 there are 7 types of raw and processed data:

1. Time series of the angle of the tank from the neutral position (in degrees, every 10 milliseconds) in a file named ‘CoolTerm_TankPosition.txt’. This data can be used as the motion input on numerical simulations.
2. Time series of the free-surface elevation in a file named ‘free_surface_heights.csv’ for each captured frame of the full tank recordings (height in pixels from bottom of the image, every 10 milliseconds). Each column spaced out by 10 pixels horizontally for a total of 232 columns.
3. Processed PIV velocities in a file named ‘PIV_velocities_corner.mat’ for each captured frame of the corner recordings. Inside this file there are velocity values along the x and y axis structured as two separate 90 $\times$ 45 matrices for every frame recorded
4. Two time series of the pressure data in files ‘digitalPressure_1.csv’ and ‘digitalPressure_2.csv’ (in millibar, approximately every 0.012 s). Each file contains pressure results from 5 sensor locations, for a total of 10. These locations are provided in the dataset

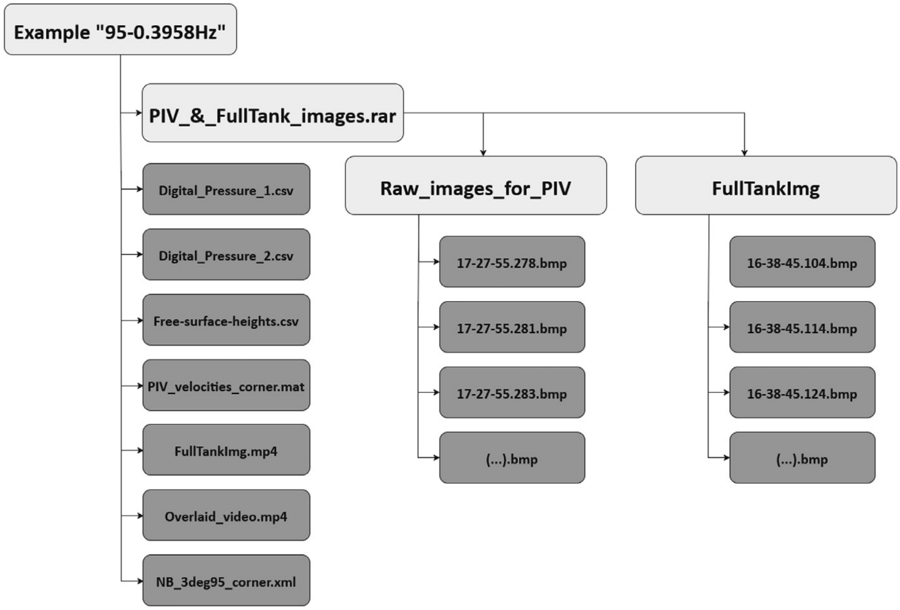

Fig. 2. Folder contents for each sloshing condition.

5. Highly compressed video of the full tank recordings named “FullTankImg.mp4”
6. Highly compressed video of the corner recordings, overlaid with the PIV vectors named “Overlaid_video.mp4”
7. Configuration file used in the PIV processing software named according to the sloshing condition. File is “.xml” type.

Given the size of the raw images folder for each experimental run (about 23Gb), it was decided to share in the dataset both the raw full tank and corner recorded images for only one sloshing condition, both with and without floating body. The chosen sloshing condition was 3 degrees of amplitude with frequency of 0.3958 Hz (motor RPM of 95). Therefore, in these specific folders the following data can also be found:

8. Raw high speed camera images of the left corner of the tank for PIV processing in files ‘*.bmp’ inside folder ‘raw_images_for_PIV’ (resolution of 1460 $\times$ 820).
9. Raw camera images of the entire tank in files ‘*.bmp’ inside folder ‘Full_tank_img’ (resolution of 2320 $\times$ 820).

For all other conditions, every type of data apart from the images is shared. Fig. 2 shows the structure and available files inside each sloshing condition folder, where the “PIV_&_FullTank_images” zipped folder is only shared for two cases.

4. Experimental Design, Materials and Methods

4.1. Tank design

The sloshing tank used in the experiments is 1 m long, 0.6 m in high, and 0.2 m wide (inner dimensions), similar to [1,2]. These dimensions were chosen in order to achieve a balance between generating significant wave height, which is critical for enhancing the accuracy and reliability of pressure readings and the available Particle Image Velocimetry (PIV) equipment and also maintaining a size that can be effectively operated by a high-power stepper motor.

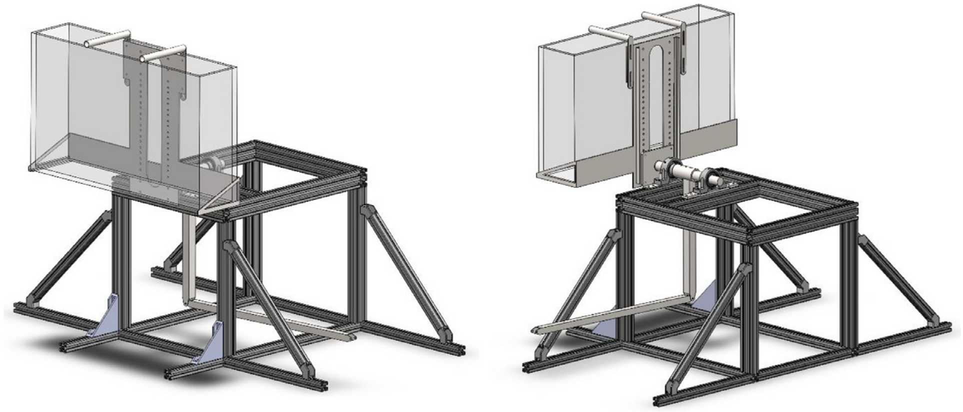

Fig. 3. Front and Backside view of the tank's overall design.

The supporting structure of the entire system was built using aluminum profile to simplify the assembly process and facilitate future addons if necessary. To prevent movement of the structure from the more aggressive sloshing conditions, the structure is bolted to the ground.

The moving parts of the system were custom made for this project. They are secured to the supporting structure through two large bearings, that support a 45 mm diameter shaft. The large diameter of this shaft ensures that the inertial forces of the sloshing fluid do not cause any torsion on the shaft, ensuring that the motor attains the specified input frequency.

The large steel backplate holding the tank was purposefully designed without covering the bottom or the sides of the tank to leave space for the pressure sensors and the LED light sheet, needed for the PIV measurements. Also, this backplate allows for the axis of rotation to be adjusted vertically to eleven positions spaced 50 mm from each other, starting with the axis of rotation on the bottom of the tank. In this dataset, all the results are with the tank on the same position, with the axis of rotation on the bottom of the tank. In Fig. 3 the 3D design of the tank's structure is shown.

The tank itself is made of 10 mm thick glass. The option to use glass instead of acrylic or polycarbonate was made for optical reasons, as glass is clearer and scratch resistant. Fifty holes were made on the tank walls (20 on the bottom plus 15 on each sidewall), and then a custom-made threaded bushing was glued on each hole, for the pressure sensors. Fig. 4 shows a schematic of the location of the threaded holes along the tank walls.

The motion of the tank is controlled by a stepper motor through a rod-crank mechanism as shown in Fig. 5. The crank in this system is a flat 12 mm thick slab of aluminium, with threaded holes for each amplitude of motion for the tank. This part allows the tank to be oscillated at amplitudes varying between 1 and 8 degrees (with 0.5° intervals, totaling 15 sloshing options).

The motor being used is a Nanotec ST8918L6708, coupled to a Nanotec 4:1 reduction gearbox, to ensure the maximum power of the motor is at the desired speeds for this project. The use of a stepper motor ensures precise control of the tank's position, and therefore precise wave generation, providing high accuracy in replicating specific wave patterns and frequencies and also allowing for the repetition of experimental runs, guaranteeing the same results. Using a more powerful regular DC motor was considered, but ultimately it wouldn't be able to provide the same precision.

Overall, the tank was designed with precision in mind and this precision is crucial for capturing detailed fluid-structure interactions, while the smaller scale of the tank maintains experimental feasibility in a controlled laboratory setting. These considerations collectively optimize the setup for accurate data collection and numerical validation. Fig. 6 shows the experimental tank prepared for an experimental PIV recording.

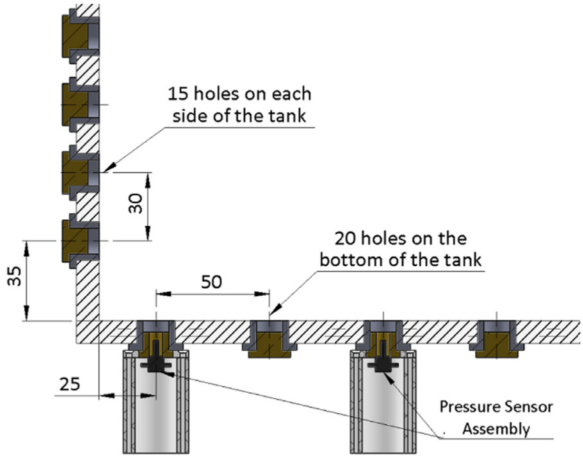

Fig. 4. Schematic of the holes for the pressure sensors.

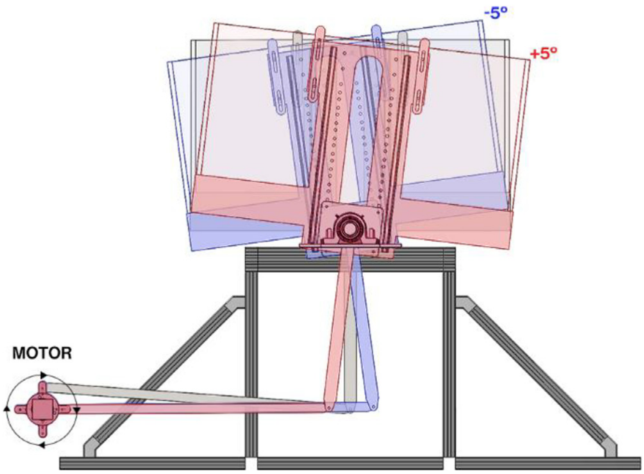

Fig. 5. Schematic of the tank's motion with the rod-crank mechanism set to 5 degrees.

4.2. Materials

As explained previously, two types of experimental runs were conducted: with and without the flexible floating body. Since the aim is to provide data to validate numerical solutions and most numerical codes include flexible bodies as made of isotropic homogeneous material, choosing the ideal material for the floating body was challenging, as the body needed to meet several criteria to ensure it could be reliably modeled in numerical simulations. The key requirements were:

1. composed from a single material; laminated materials, e.g., were ruled out to avoid complex internal structures;
2. homogenous at macroscopic scale (which excludes composites but may include material with pockets of a gaseous phase, provided that these are much smaller than the smallest dimension of the floating body), ensuring consistent behavior and being able to be accurately characterized with standard testing methods.;

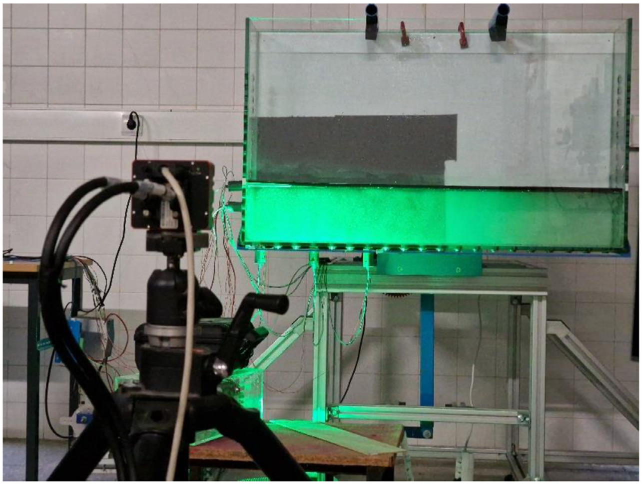

Fig. 6. Example of the sloshing tank setup ready for PIV recording.

3. less dense than water;
4. impermeable (preventing water percolation and resistant to change in properties when in contact with water);
5. appropriately flexible for the scale of the waves in the tank.

Isotropic material would be ideal, but it is not a necessary requirement. Since one of dimensions of the floating body is much smaller than the other two, it is sufficient that properties are isotropic in the plane of the two larger dimensions.

Initially, several types of rubber were considered due to their flexibility and impermeability. However, most common rubbers have density close to or above water's density and tend to be too rigid to deform under the tank's sloshing waves. But in the research for an appropriate rubber, an alternative was found: rubber foams. These are obtained through a process called foaming in which, by using a blowing agent, small gas bubbles are formed inside the rubber mixture. Two possible structures can come of this process: open or closed cell foam. Open cell resembles the common household sponge that absorbs water, and closed cell foam, which contains small, sealed cavities inside the material, preventing air and moisture penetration. This process also offers both a lower density and increased flexibility of the material.

After careful consideration, the material selected was an EPDM (ethylene propylene diene monomer rubber) closed cell rubber foam sheet, with a thickness of 8 mm. This material satisfies all the required characteristics for the floating body. However, as properties of this type of material vary greatly depending on the manufacturer and no specific properties were supplied for our sample, some tests were needed to accurately determine the material properties.

The first and most simple test is determining the density of the material. This was achieved by cutting a sample piece, measuring its mass on a high precision scale, and calculating its volume using the sample's dimensions. The density is then obtained by dividing the mass by the volume of the material.

To further characterize the mechanical properties of the EPDM rubber, especially the elasticity, the Young's Modulus (E) was determined through a series of uniaxial tensile tests. These tests were conducted on a universal testing machine (StepLab EA05). This machine is equipped with dynamic load and displacement sensors, enabling precise measurements of force and deformation.

Three tests were conducted on rectangular specimens of the material of dimensions 90 mm long, 40 mm wide (excluding grips) and 8 mm of thickness. The test specimens were clamped securely at both ends as can be observed in Fig. 7.

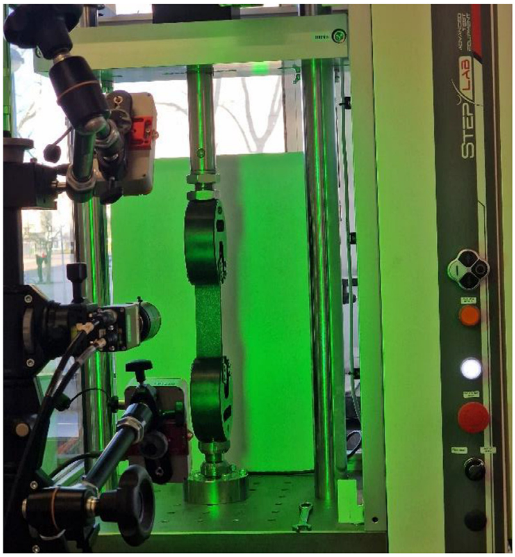

Fig. 7. Test specimen ready for tensile test with Digital Image Correlation (DIC) camera and lighting.

The test starts with the specimen fully straightened but with zero load applied. For each test, the machine stretches the material at a constant speed (1mm/s), until the maximum displacement of the machine is reached, as no fracture occured. During the test, the uniaxial tensile force applied to the specimen and the corresponding clamp movement are recorded.

In conjunction with the tensile test, a special Digital Image Correlation (DIC) camera was used to capture extensions in both x and y axis, for determining the Poisson's Ratio.

The Young's Modulus (E) and Poisson Ratio (ν) are calculated in Eq. (1):

$$E = \frac{\sigma}{\varepsilon_{transverse}}, \quad \nu = -\frac{d\varepsilon_{transverse}}{d\varepsilon_{axial}} \tag{1}$$

Where $\sigma = F/A$. Area is calculated from the dimensions of the specimen ($40mm \times 8mm$), and Force is the output of the universal testing machine. The DIC analysis provides the extensions (ε_{axial} and $\varepsilon_{transverse}$)

The elongation of the material could be calculated from the clamp's movement as $\varepsilon = \Delta L/L_0$, but Digital Image Correlation (DIC) provides more accurate extension values, so this option was chosen.

The Young's Modulus (E) can be visualized as the slope of the initial linear portion of the stress-strain curve, shown in Fig. 8, where the material has an elastic behavior. The result is the average of the three tests.

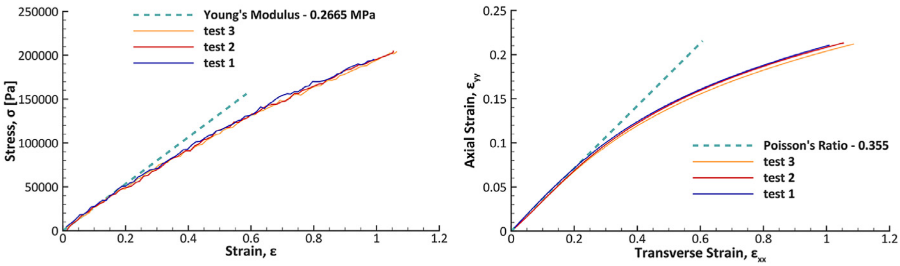

Fig. 8. Stress-strain curve with Young's modulus.

Table 1
EPDM Rubber Foam mechanical properties.

Density	Young's Modulus	Poisson's Ratio
106.27 kg/m^3	0.2665 MPa	0.355

The Poisson Ratio is also calculated as the initial slope of the three test results, shown in Fig. 8 and Table 1 shows the material properties.

4.2. Experimental procedure

For every single one of the 36 experimental conditions (18 sloshing conditions, both with and without floating body), two runs were performed. In the first run, the camera recorded the lower left corner of the tank, to acquire planar velocity vectors with PIV, and with the pressure sensors at 5 locations on the left of the tank. During the second run, the camera recorded the entire tank, and the pressure sensors repositioned to five different locations from the first run, providing pressure results for a total of 10 locations on the tank's walls and bottom.

Particle Image Velocimetry requires tracer particles to seed the fluid [6]. The seeding particles were chosen to exhibit high traceability, i.e. they should be almost neutrally buoyant and their diameter should be small. Ideally, the relative velocity between the tracer particles and the water should be in the Stokes regime. The terminal (settling) velocity ω of a tracer particle in a viscous fluid is a proxy of the relative motion. In the Stokes regime ($Re < 1$), the terminal fall velocity is

$$\omega = \frac{2}{9}\frac{\rho_p - \rho_f}{\mu} gR^2 \tag{2}$$

Where ω is the terminal velocity (m/s), ρ_p is the particle density (kg/m^3), ρ_f is the fluid density (kg/m^3), g is the gravitational acceleration (m/s^2), R is the particle radius (m) and μ is the dynamic viscosity of the fluid ($Pa \cdot s$).

The tracers are polyamide particles with a range of diameters between 60 and 80 µm Assuming values of density and viscosity for water at 20 °C and density for polyamide particles

$$\rho_f = 998.2\ kg/m^3$$

$$\mu = 1.002\ \times 10^{-3}\ Pa \cdot s$$

$\rho_p = 1.04 \cdot 998.2 = 1038.1 \frac{kg}{m^3}$ (value provided by the supplier) the sea-level value of the acceleration of gravity

$$g = 9.81\ m/s^2$$

and considering the range of tracer diameters (60 - 80 µm), one obtains $\omega = 0.08\ mm/s$ to $\omega = 0.14\ mm/s$. The particle Reynolds number is two orders of magnitude smaller than 1, which guarantees that the relative motion is indeed in the Stokes regime.

The terminal (maximum) velocity of the tracer particles is small (average 0.2 mm/s). The particles thus tend to slowly sink over time. Hence, before every experimental run for PIV analysis, the water was manually agitated to suspend any tracer particles in the bottom and obtain a homogenous seeding pattern. After this agitation, a waiting period of about 2 min is needed to achieve a still free surface and close to no movement within the fluid. The relative motion of the particles is a possible source of error in the velocity measurements but it can be shown that it is negligible if it is in the Stokes regime [5,6]. Also, checking the PIV velocity results for the first second in every run, it is concluded that the residual velocity from the manual agitation is negligible.

Each experimental run begins with the tank stationary at a neutral position (at zero degrees, bottom of the tank horizontal). After 0.5 s the sloshing motion starts and every run lasts for

36 s. This time window allows for 10 full rotations of the tank on the slowest used sloshing frequency, and a few stationary seconds at the end on the fastest frequencies.

After the recording, all necessary post processing is completed. For which the PIV configuration files and all scripts are provided with the dataset.

4.3. Data acquisition systems

The instrumentation of the tank was selected specifically for the dimensions of the phenomena observed. In this sense there are three separate data gathering systems and, in this section, a detailed overview of the hardware is provided:

1. Rotary encoder is an Autonics E50S8–1000–6-l-5 connected to an Arduino UNO, recording at a rate of 1000 Hz. The encoder has a 1000 points per revolution of resolution, meaning only about 2,8 points per degree of rotation. As this wasn't enough resolution, the encoder is connected to the tank's rotation shaft through a set of gears, totaling a gear reduction ratio of 31.25. This brings the resolution to approximately 87 points per degree of rotation (0.01152° increments).
2. The high-speed camera used is an Allied-Vision Bonito CL-400B
   - Two-dimensional two-components Particle Image Velocimetry was employed for fluid flow analysis, as the flow is essentially two-dimensional (2D). A continuous LED light sheet was used to illuminate the tracer particles only on the center plane of the tank (see green light plane in Fig. 6). The time between consecutive images was set to prevent aliasing; this resulted in an acquisition rate of 405 frames per second. The resolution used was 1460 × 820 pixels, with a region of interest comprising a third of the tank (left corner). Placing the camera further away resulted in peak-locking.
   - For the recordings of the entire tank, the of the camera acquired images at 100 frames per second and a resolution of 2320 × 820 pixels.
3. Five pressure sensors were purposefully manufactured for this tank. The sensor chosen was the Honeywell HSCDLNN100MDSA5, with a measuring range of ±100mbar. These are digital sensors connected to a Digilent Analog Discovery 2 Oscilloscope and Logic analyzer. The script used for reading the data is provided with the dataset.

Some of the raw data from the experimental runs requires further processing, such as the high-speed recordings for the PIV. The footage from the camera is processed with the in-house software QuickLabPIV, developed by [3]. It returns the two-dimensional, two-component, velocity field over time at a sampling rate of 405 Hz (the specific settings can be found in the configuration file inside the dataset folders with the example images). Also, the entire tank footage is used to determine both the free surface height (no body runs) and body deformation and height (flexible body runs) using a python script also provided with the dataset.

4.4. Repeatability of results

To ensure the reliability and precision of the experimental results for each sloshing condition, a study on the repeatability of the sloshing tank experiments was conducted. This study was essential to determine whether multiple experimental runs under identical sloshing conditions would provide the same results, both in terms of the pressure on the tank walls and velocity fields obtained from PIV. The repeatability study was crucial for validating the experimental procedure and determining whether statistical analyses were necessary to account for possible differences between runs.

For the repeatability study, five experimental runs under identical sloshing conditions were performed, each conducted on a different day to account for potential variations due to environmental factors, equipment setup, or other unknown influences. For each run, pressure measure-

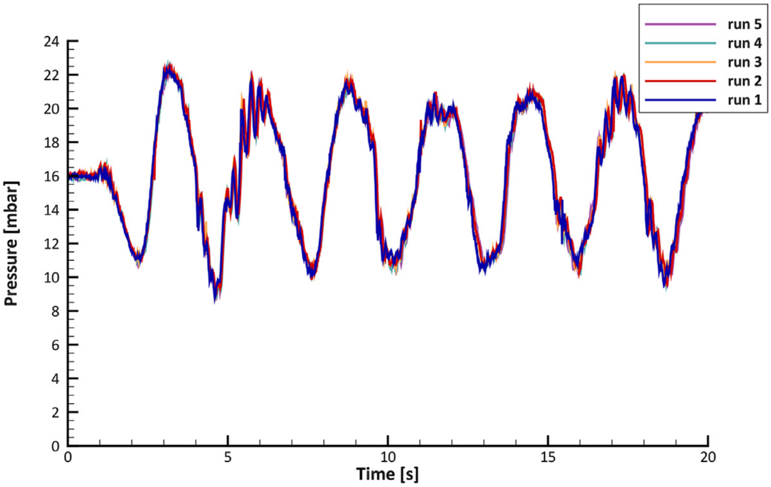

Fig. 9. Pressure results for identical sloshing conditions of 5 separate runs with the sensor located at $x = 25mm$ and $y = 0mm$.

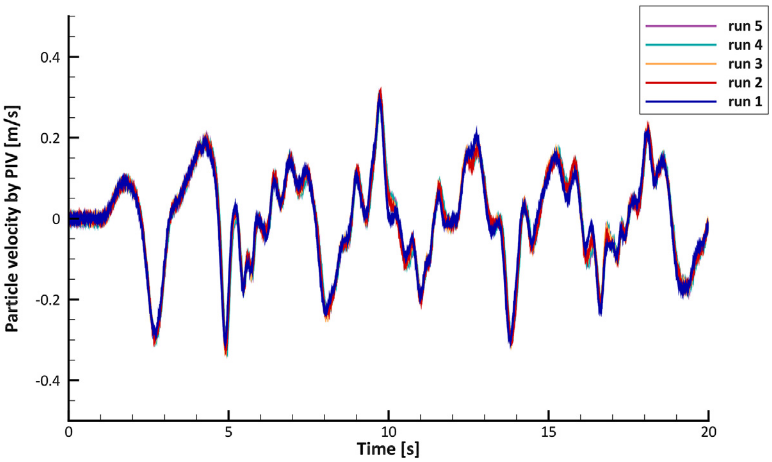

Fig. 10. Velocity results for identical sloshing conditions of 5 separate runs measured at the center of PIV image at pixel coordinates of $\boldsymbol{x} = 730$ and $\boldsymbol{y} = 420$ (position (45,90) on the PIV velocity matrix).

ments on the tank walls and velocity fields from the PIV system were recorded and analyzed and a few examples can be observed in Figs. 9 and 10.

To quantitatively analyze the repeatability of the results, Pearson and Spearman correlation coefficients were calculated between the results of the five runs for both the pressure and velocity data. The correlations between the runs were found to be exceptionally high as shown in Table 2, indicating strong agreement between the experimental measurements.

To provide a more comprehensive validation of the experiment's repeatability, supplementing the time-domain analysis, an analysis in the frequency-domain and a statistical characterization of the results was conducted.

A frequency-domain analysis was performed using Welch's method to compute the Power Spectral Density (PSD) of both the pressure and PIV velocity signals, sampled on the same locations as Figs. 9 and 10. Fig. 11 presents the overlaid PSD plots for all five experimental runs.

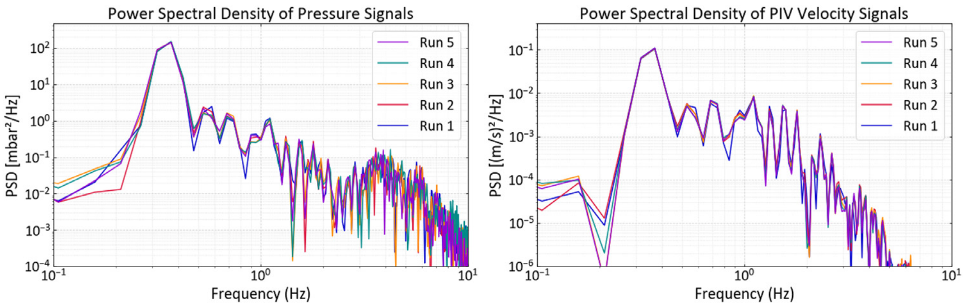

Fig. 11. Power Spectral Densities of the pressure and velocities.

Table 2
Correlation Coefficients for the repeatability study.

Correlation Coefficient	Average Value	Minimum Value
Pressure - Pearson	0.975	0.927
Pressure - Spearman	0.973	0.924
PIV - Pearson	0.960	0.876
PIV - Spearman	0.964	0.890

Table 3
Statistical analysis of the repeatability study.

Run	Pressure		PIV velocities	
	Standard deviation	Skewness	Standard deviation	Skewness
1	3.712	−0.094	0.117	−0.337
2	3.737	−0.087	0.119	−0.270
3	3.744	−0.103	0.118	−0.367
4	3.762	−0.107	0.119	−0.363
5	3.738	−0.094	0.119	−0.344

The spectra for both measured quantities show excellent agreement, with all five runs collapsing onto a single, well-defined curve. A dominant peak is clearly visible at the tank's driving frequency (0.3958 Hz). This demonstrates that the energy distribution across the relevant frequencies is highly reproducible for both the pressure and velocity fields.

For a quantitative statistical comparison, the 2nd (Standard Deviation) and 3rd (Skewness) moments were calculated. To analyze the repeatability of the primary, stable sloshing dynamics, the statistical analysis was performed on the time window between 1.1 s and 20.0 s. The results are summarized in Table 3.

The results in Table 3 show a remarkable consistency across all five runs. The standard deviation values, which represent the energy of the fluctuations, are nearly identical for both pressure and velocity. Furthermore, the skewness is also highly consistent. Together, these frequency-domain and statistical results provide strong quantitative evidence for the high fidelity and repeatability of the experimental dataset.

As a result of the repeatability study, it was concluded that the sloshing tank experiments do not exhibit significant variability between different runs, i.e. identical sloshing conditions always provide consistent and reproducible results. This allowed each sloshing condition to be performed only once during the experimental dataset creation, significantly facilitating the data gathering process while guaranteeing accurate results. Also, this repeatability analysis not only supports the reliability of the dataset but also strengthens the overall experimental methodology by demonstrating the robustness of the setup and procedures used.

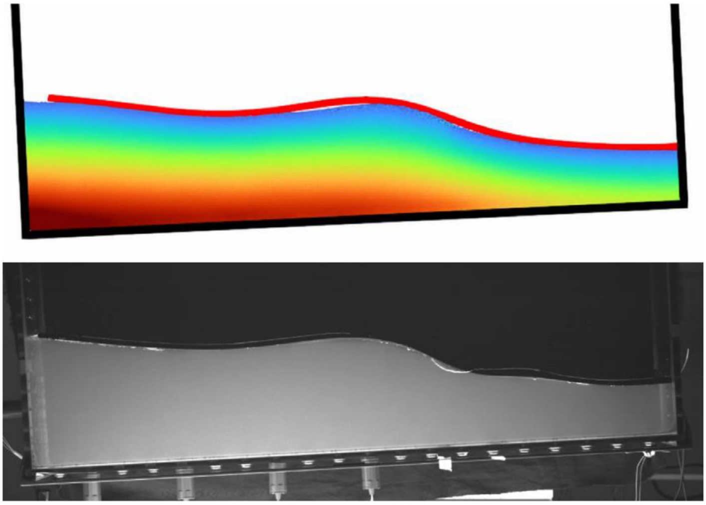

Fig. 12. Snapshot of the same instant of a numerical and experimental runs with the same sloshing conditions.

4.5. Example of application for the validation of a numerical code

To demonstrate the direct applicability and effectiveness of this dataset for numerical model validation, this section presents a brief, illustrative comparison between the experimental data and a numerical simulation performed with the open-source Smoothed Particle Hydrodynamics (SPH) code DualSPHysics [4]. The chosen case corresponds to the sloshing condition with the flexible floating body, an oscillation amplitude of 3 degrees, and a frequency of 0.3958 Hz. The numerical model was configured to replicate the experimental setup, using the provided tank motion data as input and the measured material properties for the flexible body.

A primary step in any validation process is the qualitative visual comparison of the overall system dynamics. Fig. 12 presents a side-by-side comparison of a snapshot from the high-speed camera recording and the corresponding instant from the DualSPHysics simulation. A good visual agreement is observed, particularly in the deformation of the flexible body and the shape of the

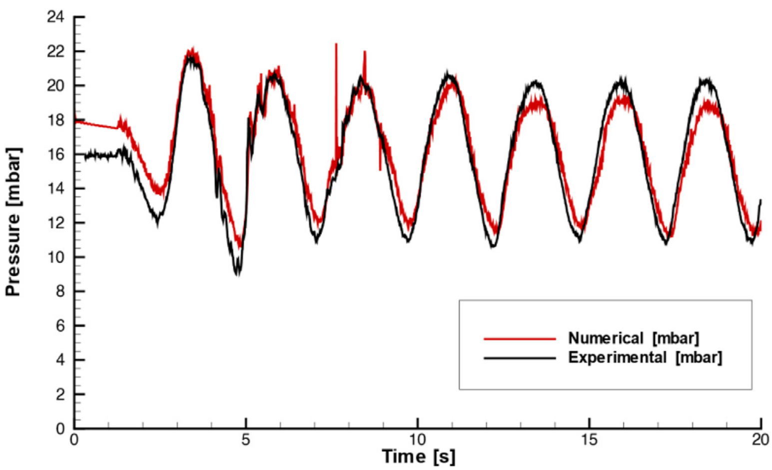

Fig. 13. Pressure comparison between numerical and experimental results.

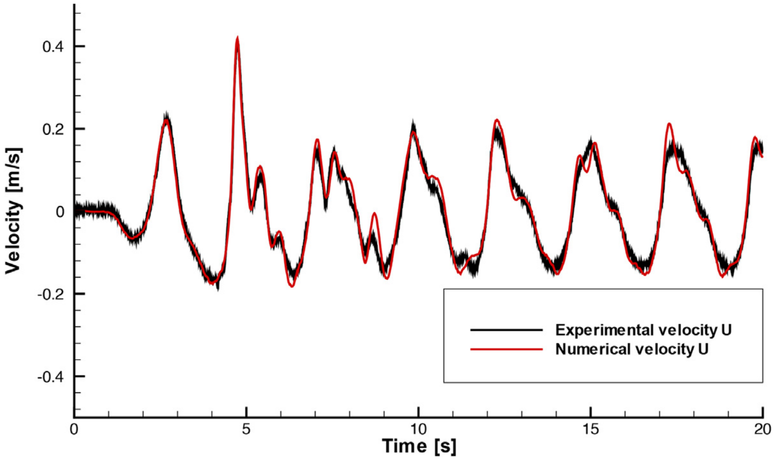

Fig. 14. Velocity comparison between numerical and experimental results.

free surface, indicating that the numerical model is capable of capturing the main features of the fluid-structure interaction.

Following a visual assessment, quantitative comparisons are performed using the time series data. Fig. 13 shows the comparison between the numerically obtained pressure results and the experimental signal at the leftmost sensor located on the bottom of the tank ($x = 0.025$ m, $y = 0$ m). The numerical model successfully reproduces the phase and the amplitude of the pressure peaks, showing strong agreement with the experimental measurements.

Finally, to validate the code's ability to predict the dynamic fluid flow, the velocity field is also compared. Fig. 14 compares the time series of the horizontal velocity component (u) at a point within the fluid domain ($x = 0.175$ m, $y = 0.065$ m). Once again, the numerical results align well with the PIV data from the experiment, capturing both the timing and magnitude of the velocity fluctuations. This brief example demonstrates the comprehensive nature of the dataset, which allows for a multi-faceted validation of a numerical code's performance, from visual dynamics to local pressure and velocity fields.

Limitations

The authors would like to have included the high-speed recordings for every sloshing condition, however this would have resulted in a dataset too large to keep in the available online data repositories.

Ethics Statement

This study does not involve human subjects, animal experiments or any data collected from social media platforms. Therefore, we confirm that our research strictly adheres to the guidelines for authors provided by Data in Brief in terms of ethical considerations.

Data Availability

Experimental Dataset on the interaction of sloshing tank waves with a flexible floating body (Original data) (Zenodo).

CRediT Author Statement

Francisco Bernardo: Methodology, Software, Validation, Investigation, Data curation, Writing – original draft, Visualization; **Moisés Brito:** Conceptualization, Resources, Writing – review & editing, Supervision, Funding acquisition; **Rui M.L. Ferreira:** Conceptualization, Resources, Writing – review & editing, Funding acquisition; **João Leal:** Conceptualization, Writing – review & editing, Supervision.

Acknowledgements

The author gratefully acknowledges the financial support provided by the Portuguese Foundation for Science and Technology (FCT), which funded the main author's PhD scholarship (2021.05392.BD). Special thanks are extended to NOVA School of Science and Technology and Instituto Superior Técnico for their invaluable contributions, including funding most of the construction of the experimental facility and providing the necessary instrumentation for this study. Their support and resources were instrumental in achieving the outcomes presented in this dataset.

Declaration of Competing Interest

The authors declare that they have no known competing financial interests or personal relationships that could have appeared to influence the work reported in this paper.

References

[1] A. Souto-Iglesias, E. Botia-Vera, A. Martín, F. Pérez-Arribas, A set of canonical problems in sloshing. Part 0: experimental setup and data processing, Ocean Eng. 38 (16) (November 2011) 1823–1830, doi:10.1016/j.oceaneng.2011.09.008.

[2] L. Delorme, A. Colagrossi, A. Souto-Iglesias, R. Zamora-Rodríguez, E. Botía-Vera, A set of canonical problems in sloshing, part I: pressure field in forced roll—Comparison between experimental results and SPH, Ocean Eng. 36 (2) (February 2009) 168–178, doi:10.1016/j.oceaneng.2008.09.014.

[3] L.P. Mendes, A.M. Ricardo, A.J. Bernardino, R.M. Ferreira, A hybrid PIV/optical flow method for incompressible turbulent flows, Water. (Basel) 16 (7) (April 2024) 1021, doi:10.3390/w16071021.

[4] A.J.C. Crespo, J.M. Domínguez, B.D. Rogers, M. Gómez-Gesteira, S. Longshaw, R. Canelas, R. Vacondio, A. Barreiro, O. García-Feal, DualSPHysics: open-source parallel CFD solver based on smoothed particle hydrodynamics (SPH), Comput. Phys. 4 Commun. 187 (2015) 8–28.

[5] R.M.L. Ferreira, R. Aleixo, M. In Muste, D.A. Lyn, D. Admiraal, R. Ettema, V. Nikora, M.H. GarciaLaser-Doppler Velocimetry/Anemometry, Experimental hydraulics: methods, instrumentation, Data Processing and management: Volume I: Fundamentals and methods. IAHR Monographs, Chapter 3.6, II, CRC Press, Taylor and Francis Group, 2017 ISBN 9781138027534 - CAT# K25651.

[6] J. Westerweel, R.J Adrian, Particle Image Velocimetry (No.30), Cambridge university Press, 2011.